

Detailed analysis of the direct piezo-response of AlN nanowire-based vertically integrated nanogenerators

N. Buatip¹, T. Auzelle², P. John², S. Rauwerdink², M. Sohdi¹, M. Saluan¹, B. Fernandez¹, E. Monroy³, D. Mornex¹, C. R. Bowen⁴
R. Songmuang^{1,*}

¹ Université Grenoble Alpes, CNRS, Grenoble INP, Institut Néel, 38000 Grenoble, France

² Paul-Drude-Institut für Festkörperelektronik, Leibniz-Institut im Forschungsverbund Berlin e.V. Hausvogteiplatz 5-7, 10117 Berlin, Germany

³ Université Grenoble-Alpes, CEA, Grenoble INP, IRIG, PHELIQS, F-38000, Grenoble, France

⁴ Department of Mechanical Engineering, University of Bath, BA2 7AY Bath, UK

*Corresponding author: rudeesun.songmuang@neel.cnrs.fr

In this work, detailed analysis of the direct piezo-response of AlN nanowire-based vertically integrated nanogenerators (VINGs) is undertaken as a function of mechanical excitation frequency. We demonstrate that the piezo-charge, piezo-voltage, and impedance of the devices can be directly correlated using an equivalent circuit model. The performance figure of merit (FoM) of nanowire-based VINGs, namely the piezoelectric voltage constant (g) for sensing, and the product $g \cdot d$ for energy harvesting, where d is a piezoelectric charge constant, are extracted from our presented results and compared with that of bulk single crystal GaN and quartz substrates, as well as sputtered AlN thin films. The measured FoM values suggest that the nanowires can outperform their rigid counterparts in terms of mechanical sensing applications, while further improvements are required to enhance their capability for energy generation. This work not only provides new experimental guidelines for understanding the direct piezo-characteristics of VINGs, but it also enables a quantitative comparison between nanostructured piezoelectric devices fabricated using different materials or architectures.

1. Introduction

Nanostructured piezoelectric energy harvesters, namely, nanogenerators, which convert ambient mechanical energy into electrical energy have become a research hotspot in recent decades. This type of device holds great promise for driving low-power electronics and/or serving as a self-powered sensor for future self-sustained and smart systems^{1,2}. In this regard, wurtzite piezoelectric semiconductors (such as ZnO and III-N) produced in the form of nanowires are among the promising active elements for nanogenerators due to their superior flexibility and strain sensitivity compared to traditional high stiffness, and brittle piezoelectric materials. In contrast to the extensively studied ZnO and GaN nanowires, AlN nanowire-based nanogenerators have not been widely explored despite their potential advantages. Notably, AlN is a highly insulating material due to its large bandgap of 6.2 eV³, which can minimize screening effects that generally occur in unintentionally n-type doped ZnO. In addition, the wide-bandgap AlN material exhibits the highest piezoelectric coefficients among the group-III nitrides^{3,4}, which is a critical parameter for piezoelectric sensors and energy harvesters. The attractive intrinsic material properties of AlN, combined with the mechanical flexibility of nanowires, is expected to substantially enhance the performance of nanowire-based nanogenerators.

Despite a growing body of literature that reports an increase in signal output from nanogenerators using a variety of nanomaterials and architectures, the ability to accurately evaluate and compare these devices remains a topic of ongoing discussion^{5,6,7}. This is attributed to the often-limited details of in-house measurement setups used in the literature and the absence of a standardized characterization protocol. The detected signals of nanogenerators are typically in the form of voltage and current spikes, which are produced during rapid impulsive pressing or bending of the piezoelectric devices^{1,Error! Bookmark not defined.,8,9,10}. While such measurements can offer useful information related to device efficiency, they usually cannot fully provide a comparable description of performance and operational characteristics. For example, unlike the voltage signal, few groups have paid attention to measuring the generated piezoelectric charge^{11,12}, even though it is the primary output and a crucial evaluation metric¹³. Furthermore, to assess their potential applications and integration

compatibility with other electronic components, more detailed analyses of the piezoelectric response are required¹⁴.

Here, we perform detailed investigations on the direct piezo-response characteristics of AlN nanowire-based vertically integrated nanogenerators (VINGs). Our characterisation setup is designed based on the Berlincourt principle¹⁵, which is used in commercial systems for measuring the piezoelectric charge coefficients of materials^{16,17,18}. The Berlincourt concept involves applying a controlled force to the device under test (DUT) and detecting its mechanically induced electrical signal. The piezoresponse (i.e., charge and voltage) are investigated as a function of frequency of mechanical excitation. Electrical measurements, such as current-voltage and impedance analyses, are also carried out to gain an insight into the resistance and capacitance of the devices. The obtained data are used for constructing an equivalent circuit that quantitatively describes the direct piezoelectric response behaviours. The advantage of our setup is that the piezo-charge, piezo-voltage, and device impedance are measured at the same position of the device, thereby greatly facilitating signal interpretation and the correlation of each property. Such studies have rarely been reported to date.

To ensure the reliability and accuracy of the experimental setup, we first analyse the piezo-response of a well-known reference single crystal piezoelectric material, namely a wurtzite GaN substrate and an x-cut quartz. We also investigated a sputtered polycrystalline AlN thin film on Si substrate for comparison. Subsequently, we applied our measurement protocol to evaluate GaN and AlN nanowires which are encapsulated in a polymer and fabricated into a VING architecture¹⁹. We demonstrate that a classical equivalent circuit model for piezo-sensing devices can effectively capture the characteristics of the piezoelectric response of nanowire-based VINGs. From our measurements, we can extract the piezoelectric voltage constant (g) and the product $d \cdot g$ which represents the figure of merit (FoM) for piezoelectric sensors and energy harvesters, respectively^{20,21,22}, where d is the piezoelectric charge constant. Our observations reveal that the g coefficient of the AlN nanowire-based VINGs exceeds that of the conventional reference samples, indicating the superior suitability and advantages of the nanowires for mechanical sensing applications.

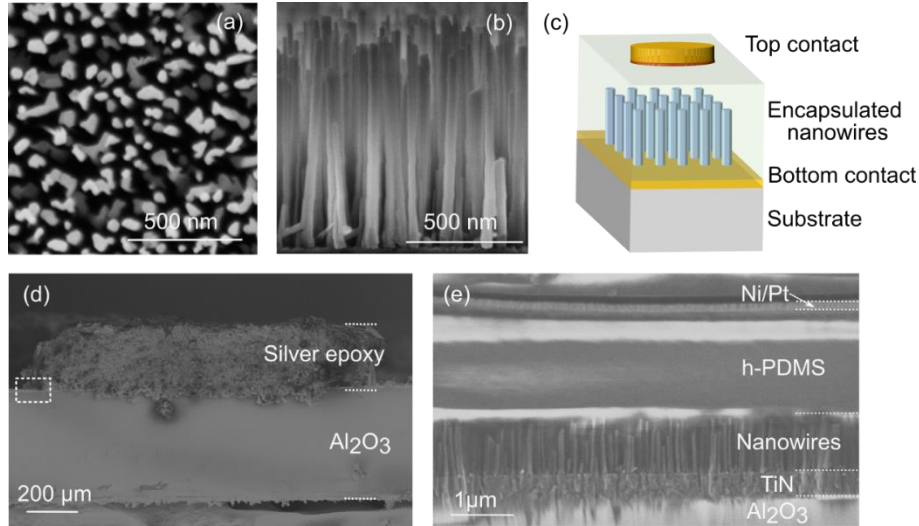


Figure 1: (a) Top and (b) side view SEM images of the as-grown AlN nanowires. (c) Schematic of the nanowire-based VINGs structure (schematic is not to scale.). (d) Side view SEM image and (e) zoomed-in image of the square area in (d) of AlN nanowire-based VINGs.

However, when considering the $d \cdot g$ value which represents the volume density of generated energy due to an applied stress. The results suggests that the AlN nanowire-based VINGs can provide a power output comparable to that of the reference materials, indicating untapped potential for further enhancement.

2. Experimental details

2.1 Nanowire growth and device fabrication

To investigate single crystal piezoelectric materials, a (0001) Fe-doped GaN semi-insulating substrate ($6 \times 10 \text{ mm}^2$) with a thickness of $475 \pm 0.25 \text{ } \mu\text{m}$ was purchased from Kyma Technology. The resistivity of the substrate was $>10^6 \text{ } \Omega\text{-cm}$. For the x-cut quartz, a substrate ($10 \times 10 \text{ mm}^2$) with a thickness of $500 \text{ } \mu\text{m}$ was purchased from MTI corporation. For the characterizations of piezoelectric thin film, an AlN layer with a thickness of 300 nm was sputtered on highly doped Si(111) substrate using radio-frequency-magnetron sputtering at $300 \text{ } ^\circ\text{C}$. A $10\text{-nm Ti}/100\text{-nm Au}$ layer was deposited on the sample surface to serve as an electrical contact.

In the case of the nanowire-based devices, vertically aligned Al-polar AlN and N-polar GaN nanowires were grown using plasma-assisted molecular beam epitaxy (PAMBE). The Al-polar AlN nanowires were grown on a 400 nm TiN buffer layer on a (0001) sapphire substrate. The TiN is highly conductive and functions as a bottom electrode for the nanowire devices. Exact details of their growth and structural analyses are described elsewhere^{23,24,25}. The polarity of the nanowires was verified by piezo-response force microscopy²⁶ and transmission electron microscopy on the samples grown under identical conditions^{24,27}. The N-polar GaN nanowires were grown on a highly doped n-type Si(111) substrate, with a thin AlN buffer layer. In this case, the conductive Si substrate was used as the bottom contact of the nanowires. Both types of nanowires have diameters and lengths in the range of $50\text{-}100 \text{ nm}$ and $500\text{-}1000 \text{ nm}$, respectively, with nanowire densities ranging from 10^9 to 10^{10} cm^{-2} , as determined using scanning electron microscopy (SEM). Figures 1(a)-(b) show typical top and side view SEM images of the as-grown AlN nanowires.

To investigate and characterise the direct piezo-response of the nanowire ensemble, we fabricated a conventional nanowire VING structure, as shown in the schematic in Figure 1(c). The surfaces

of GaN and AlN nanowires were cleaned using oxygen plasma via a PLASSYS reactive ion etching system (10 W for 15 seconds). Subsequently, the nanowires were encapsulated in a hard-polydimethylsiloxane (h-PDMS)²⁸ using a spin coating technique. The samples were then baked at $80 \text{ } ^\circ\text{C}$ for 30 minutes under a vacuum of 90 mbar . Before electrode deposition, the encapsulated layer was activated using oxygen plasma (10 W for 15 seconds) to enhance the bonding between the h-PDMS and metal contact²⁹. Then, a $5\text{-nm Ni}/100\text{-nm Pt}$ layer was evaporated onto the sample to serve as a top electrode. Subsequently a silver epoxy (M.G. Chemicals, 8330D) with a thickness of a few hundred micrometres was covered over the top electrode to improve device stability. Figures 1(d)-(e) show large-scale and zoomed-in SEM images of AlN nanowire-based VINGs. The latter image shows a $2\text{-}\mu\text{m}$ thick layer of h-PDMS remaining on top of the encapsulated nanowires.

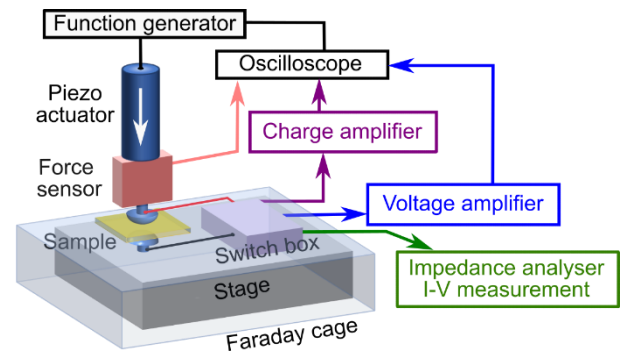


Figure 2: Schematic of the measurement setup for piezo-voltage, piezo-charge, and electrical characteristics of the piezoelectric devices.

2.2 Direct piezo-response measurements and electrical characterisation

A schematic of our measurement setup is shown in Figure 2, where a dynamic force with a controlled frequency and waveform was applied to the DUTs through a piezoelectric actuator (Physik Instrumente, PI840.30). The applied force was measured using the force sensor (Futek LSB201). We applied a sinusoidal force for excitation, where $F(t)$ is represented by $F(f, t) = F_{dc} + F_{ac} \cdot \sin(2\pi f \cdot t + \phi_F)$, where f and ϕ_F are the frequency and phase of

the excitation, respectively. The amplitude of the applied force (F_{ac}) ranges from 300 to 500 mN, while an excitation frequency (f) was swept from 0.3 to 150 Hz. A preload (F_{dc}) was applied that was between 2 and 4 N to ensure electrical and mechanical stability. This preload does not affect the dynamic piezoelectric response characteristics of the rigid samples.

The electronics for piezo-response signal acquisition consisted of a charge amplifier (Kistler 1505A) with an operating frequency that ranged from 0.16 Hz to 30 kHz and a low-frequency voltage amplifier with an input resistance (R_{in}) of 1 T Ω and an input capacitance (C_{in}) of 18 pF (FEMTO, DLPVA-100-F), which can be operated from DC to 200 kHz. After detection and measurement of the piezoelectric signal, an impedance measurement was performed at the same position under the same static preload using an LCR meter (Keysight 4980AL) with an excitation voltage of 2 V and frequency ranging from 20 Hz to 1 MHz. The capacitance (C_{pz}) and resistance (R_{pz}) values of the DUTs were measured using the parallel equivalent circuit model. The current-voltage (I - V) characteristics of the DUTs were measured using a source meter unit (Keithley 2636B). The DC resistance (R_{dc}) was derived from the I - V curve obtained by applying the bias ranging from -1 V to +1 V.

3. Results and discussion

3.1 Piezoelectric response of a reference GaN bulk substrate

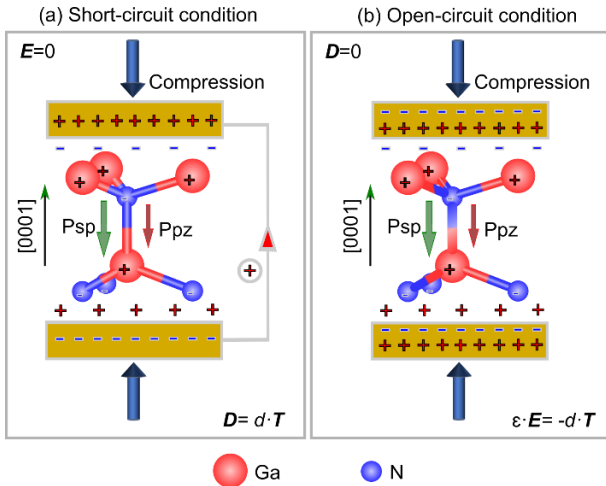


Figure 3 Schematics illustrating a Ga-polar GaN crystal subjected to a compressive force along its c -axis under (a) short-circuit and (b) open-circuit conditions.

Figures 3(a)-(b) illustrate the crystal structure of wurtzite GaN and its corresponding polarization. As a polar crystal, GaN exhibits a spontaneous polarization (P_{sp}), an inherent polarization that occurs at zero external stress. The sign of P_{sp} of Ga-polar GaN is *negative* in the [0001] direction. When an external stress (T) is applied, the centres of symmetry of the positive and negative ions shift further away from each other, thereby generating a piezoelectric polarization $P_{pz} = d \cdot T$. The applications of a compressive stress along the c -axis of the Ga-polar GaN crystal induces a *negative* P_{pz} ^{3,4}. Following the constitutive equation for a direct piezoelectric effect^{30,31}, the electric displacement (D) is described by equation (1) as follows.

$$D = \epsilon \cdot E + d \cdot T \quad (1)$$

where E is the electric field within the material and ϵ is the material dielectric permittivity. Under a short-circuit condition ($E = 0$), equation (1) is reduced to $D = d \cdot T$. In this scenario, P_{pz} is compensated by the electric field from the true charges on the electrode, resulting in the vanishing of the resultant field in the material; see Figure 3(a). In contrast, no true charge appears on the electrodes under open-circuit conditions ($D = 0$), as shown in Figure 3(b). Hence, the electric field from the surface charges in the piezoelectric crystal follows the relation: $\epsilon \cdot E = -d \cdot T$.

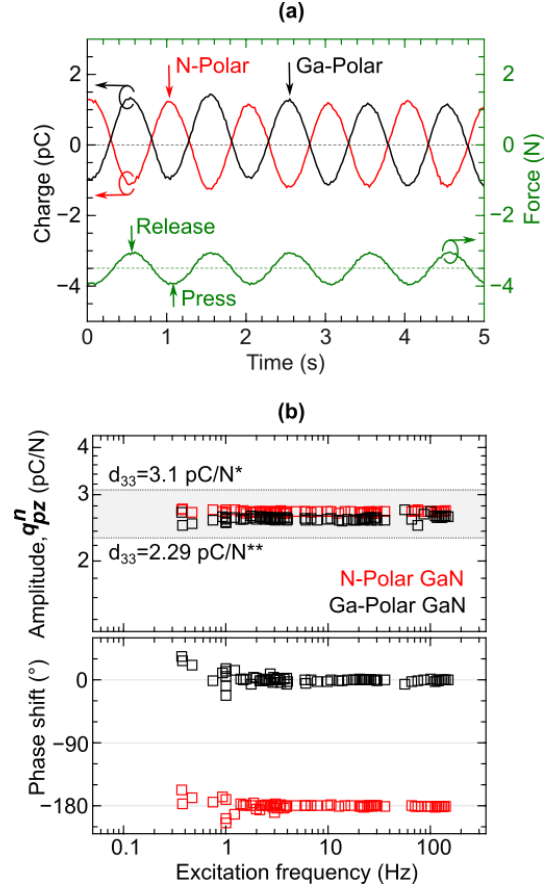


Figure 4: (a) Charge signals from the Ga- and N-polar surfaces of a GaN semi-insulating substrate during a sinusoidal force excitation at 1 Hz, shown in black and red solid lines, respectively. (b) Corresponding normalized charge amplitude (q_{pz}^n) and phase response as a function of excitation frequency from 0.3 to 150 Hz. Grey shade represents the range of d_{33} of GaN from the literature, namely $d_{33} = 3.1 \text{ pC/N}^*$ ³² and $d_{33} = 2.29 \text{ pC/N}^{**}$ ⁴

The value and sign of P_{pz} can be deduced from the charges flowing through the external circuit, e.g. using voltage or charge amplifiers^{13,13,15,33}. In the charge detection circuit, an operational amplifier (op-amp) compensates for the generated piezoelectric charges in the DUTs by charging the feedback capacitance to maintain a zero-voltage difference between the two input terminals, thus applying the short circuit condition (see also Figure S1 in supplementary information). In our measurement configuration, the force is exerted in the z -direction along the c -axis of the GaN substrate. Considering only the dynamic response, the electrical displacement (D_z) in the time domain can be quantified by equation (2).

$$D_z(t) = \frac{d_{33,eff}}{A_F} \cdot F(t) = \frac{Q_z(t)}{A_Q} \quad (2)$$

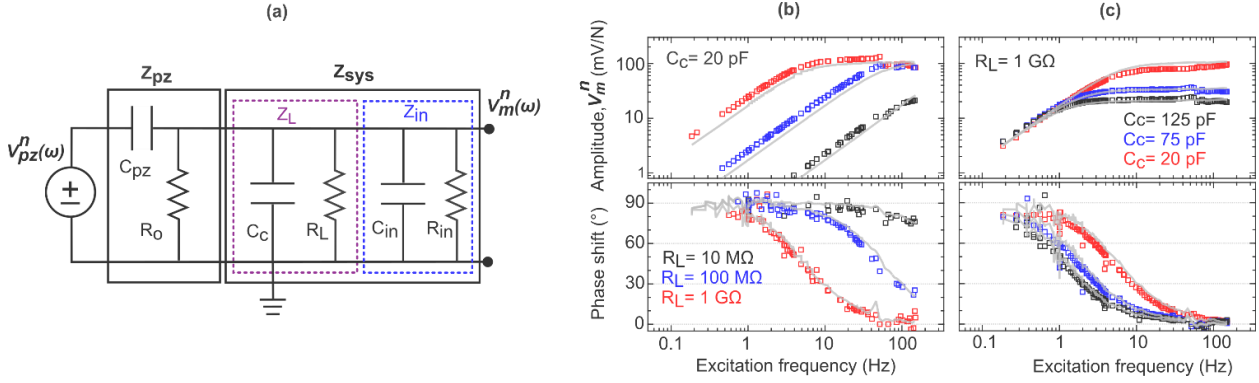


Figure 5: (a) Equivalent circuit of a piezoelectric material connected to a voltage detection circuit. C_{in} and R_{in} of the voltage amplifier are 18 pF and 1 T Ω , respectively, while C_{pz} and R_o of the studied DUTs are presented in Table 1. (b)-(c) Normalized voltage amplitude and phase response from Ga-polar GaN semi-insulating substrate measured using various R_L and C_c . Grey solid lines in (b) and (c) represent the amplitude and the phase response calculated from the equivalent circuit in (a), using $C_{pz} = 8$ pF and $R_o > 10$ G Ω .

where A_F is the area where the force is applied, and A_Q is the area where the charges are developed. These areas are generally of the same size. The parameter $Q_z(t)$ is the generated piezoelectric charge on the <0001> surface of the GaN, while $d_{33,eff}$ is the effective piezoelectric charge coefficient along the stressed direction. As the excitation frequency is sufficiently low, we can impose a quasi-static condition. The $d_{33,eff}$ is determined by dividing the charge amplitude with the force amplitude^{17,18}.

Figure 4(a) presents the charge signals from the Ga- and N-polar surfaces of a GaN semi-insulating bulk substrate, measured using the charge amplifier. The sinusoidal force excitation, represented by the green solid line, has an amplitude (F_{ac}) of 440 mN and a frequency (f) of 1 Hz. The minimum point of the force signal represents the compressive force on the sample surface generated by the piezo-actuator, whereas the maximum force related to when the piezo-actuator was released from the substrate. The negative DC offset in the force signal results from the application of a preload of 3.5 N that presses on the sample surface during the measurement.

The black solid line curve in Figure 4(a) reveals that *negative* charges were generated on the *Ga-polar* surface of the GaN substrate when a *compressive* force was applied. Conversely, *positive* charges appear when the force was released from the surface. When the sample was *physically* inverted, *positive* charges were detected under the *compressive* force on the *N-polar* surface. This observation is consistent with the sign of P_{pz} of GaN, thereby evidencing the piezoelectric nature of the signals. Substrate bending which could strongly influence the piezoelectric signal^{26,34}, is ruled out since the force is applied symmetrically on both sides of the samples.

Figure 4(b) illustrates the charge signal analysed in relation to the mechanical excitation and plotted as a function of frequency, ranging from 0.3 to 150 Hz. The upper panel of this figure shows the charge amplitude normalized by the force amplitude (q_{pz}^n), corresponding to the $d_{33,eff}$ of the investigated GaN substrate. The obtained $d_{33,eff}$ of 2.7 pC/N remains constant within our excitation frequency range and falls within the range of values reported in the literature^{4,32,35}. The phase shift is calculated by $\Phi_Q - \Phi_F$, where Φ_Q is the phase of the charge signal, and Φ_F is that of the mechanical excitation. The lower panel of Figure 4(b) shows the 0° and 180° phase-shift for the Ga-polar and N-polar surfaces of GaN substrates, respectively, confirming our interpretation of

Figure 4(a). Our measurements on an x-cut quartz substrate (Figure S2 in supplementary information) also provide a $d_{11,eff}$ of 2.23 pC/N, which is again consistent with the value reported in the literature^{22,36}. The results are summarized in Table 1.

For the piezoelectric voltage measurement, the signal was detected through a load resistor, R_L , which was placed at the input terminals of a voltage amplifier. The piezoelectric material is modelled as a voltage generator connected with a capacitance (C_{pz}) and a dissipative resistive loss (R_o)³⁷. The interfacing cable is represented by the capacitance C_c . During a measurement, the finite input impedance (Z_{in}) of the op-amplifier must be considered in the equivalent circuit, as presented in Figure 5(a)^{38,39}. The variation of the impedance of the voltage detection circuit can significantly affect the detected voltage signal at different frequencies, unlike the case for charge detection¹³. For this reason, the absolute values of piezo-voltages cannot be used as an indicator of device performance without details of testing configurations.

The detected voltage normalized with the force amplitude ($V_m^n(\omega)$) is related to the voltage generated by the DUTs ($V_{pz}^n(\omega)$) through the transfer function $H(\omega)$ as follows:

$$V_m^n(\omega) = H(\omega) \cdot V_{pz}^n(\omega) \quad (3)$$

where $\omega = 2\pi f$ and $H(\omega) = \frac{Z_{sys}}{Z_{sys} + Z_{pz}}$ Z_{sys} is the total impedance of the detection circuit, and Z_{pz} is the impedance of the DUTs.

We experimentally demonstrate the dependence of the piezoelectric voltage on the measurement configuration by varying R_L up to 1 G Ω and C_c up to 125 pF where C_c is the capacitance corresponding to the interfacing coaxial cable and has the value of 100 pF/m. The normalized voltage amplitude ($V_m^n(\omega)$) and phase response, shown in Figures 5(b)-(c), reveal the characteristic of a high-pass filter, in which the voltage signals with frequencies below a cut-off frequency ($f_{cut-off}$) are attenuated, and their phase becomes 90°, thereby leading the mechanical excitation. Above $f_{cut-off}$, the amplitude reaches a saturation value. In agreement with the behaviour of the charge signal shown in Figure 4(b), the voltage signal is in-phase with the mechanical excitation for the Ga-polar GaN substrate, while it exhibits a 180° shift for the N-polar substrate (not shown). It should be noted that $f_{cut-off}$ is determined by the RC time constant of the entire circuit.

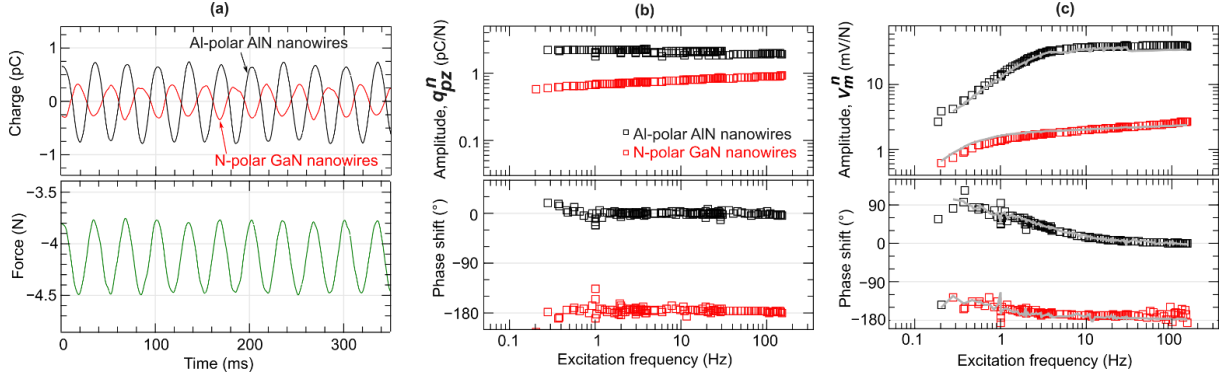


Figure 6 (a) Charge signal (upper panel) obtained from nanowire-based VINGs, i.e., N-polar GaN nanowires (GaN-NW-01) and Al-polar AlN nanowires (AlN-NW-01), subject to a sinusoidal force excitation of 30 Hz (lower panel). (b) Charge and (c) voltage responses, i.e., normalized amplitude (upper panel) and phase (lower panel), as a function of excitation frequency ranging from 0.3 to 150 Hz. Grey solid lines in (b) and (c) represent the values derived from the equivalent circuit in Figure 5(a), utilizing the device parameters specified in Table 1.

The normalized piezoelectric charge and voltage signals as a function of frequency can be correlated with the equivalent circuit shown in Figure 5(a) by the following relation:

$$V_{pz}^n(\omega) = \frac{q_{pz}^n(\omega)}{C_{pz}} \approx \frac{2.7}{8} = 0.337 \text{ V/N} \quad (4)$$

We apply equation (3) to deduce $V_m^n(\omega)$ from $V_{pz}^n(\omega)$, considering the impedances of the detection system and the DUTs. Through impedance analyses of the GaN bulk substrate, we obtain a relatively constant capacitance (C_{pz}) of 8 pF up to 1 MHz, with a tangent loss of less than 0.1. The I - V characteristic shows a DC resistance (R_{dc}) higher than 10 G Ω , which is interpreted as R_o in the equivalent circuit. The parameters of our detection circuit are $C_c = 2$ pF, $R_L = 1$ G Ω , $C_{in} = 18$ pF, and $R_{in} = 1$ T Ω . The derived $V_m^n(\omega)$ is plotted as grey solid lines in Figures 5(b)-(c), aligning with the amplitude and phase of the piezo-voltage response from all measurement configurations. The normalized saturation voltage (V_{sat}^n) obtained above the cut-off frequency can also be estimated by equation (5).

$$V_{sat}^n = \frac{C_{pz}}{C_{pz} + C_c + C_{in}} \cdot V_{pz}^n = \frac{q_{pz}^n}{C_{tot}} \quad (5)$$

where $C_{tot} = C_{pz} + C_c + C_{in}$.

3.2 Direct piezoresponse analyses of N-polar GaN and Al-polar AlN nanowire-based VINGs

In this section, we employ the measurement protocol outlined in Section 3.1 to investigate the piezoelectric signals emanating from III-Nitride nanowire-based VINGs. To mitigate the issue of device instability arising from the soft-nature of the PDMS-nanowire composite layer, we enhanced its structural stability and stiffness by covering the top electrode with a thick and more rigid layer of silver epoxy. All presented devices possess stable characteristics for over 10,000 cycles across the entire range of excitation frequencies up to 150 Hz. This robust performance ensures our reliable analyses.

Table 1: Comparison of the measured $d_{33,eff}$ and V_{sat} , including electrical parameters (i.e., C_{pz} , C_{tot} , R_{pz} , and R_{dc}) of the studied DUTs, such as Ga-GaN semi-insulating substrate, x-cut quartz, sputtered AlN thin films as well as N-polar GaN and Al-polar AlN nanowire-based VINGs. The extracted values of $C_{tot} \cdot V_{sat}$, V_{pz}^n , V_{sat}^n , $g_{33,eff}$, and $g_{33,eff} \cdot d_{33,eff}$ are also summarized. Theoretical values of d_{33} , g_{33} and the product $d_{33} g_{33}$ of AlN single crystal are also presented for comparison.

Device under test (DUTs)	C_{pz}	C_{tot}	R_{pz}	R_{dc}	$d_{33,eff}$	$C_{tot} \cdot V_{sat}$	V_{pz}^n	V_{sat}^n	$g_{33,eff}$	$g_{33,eff} \cdot d_{33,eff}$
	pF		Ω		pC/N		mV/N		$\times 10^{-3}$ Vm/N	$\times 10^{-15}$ m ² /N
Ga-GaN	8	28	>10G	>10G	2.70	2.80	337	100	29.3	79.11
x-cut quartz*	10	30	>10G	>10G	2.23	1.95	223	65	55.5	123.77
AlN (theoretical) ⁴	-	-	-	-	5.35	-	-	-	66.1	353.64
Sputtered AlN	7	27	1 G	>10G	0.90	1.00	129	37	11.1	9.99
GaN-NW-01**	365	385	140M	>10G	0.84	0.80	2.2	2.2	31.6	26.54
AlN-NW-01	37	57	>10G	>10G	2.34	2.22	63.2	39	88.1	206.15
AlN-NW-02	57	77	>10G	>10G	2.17	2.09	38.1	27.1	81.7	177.29
AlN-NW-03	26	46	>10G	>10G	1.27	1.20	48.8	26.5	47.8	60.71
AlN-NW-04	77	97	1.5G	8.5G	0.90	0.80	11.6	7.5	33.9	30.51
AlN-NW-05**	255	275	260M	1.3G	0.75	0.77	2.9	3	28.2	21.15
AlN-NW-06**	285	305	15M	2.2M	0.65	0.60	2.3	2	24.5	15.93

* For x-cut quartz, the $d_{11,eff}$ is measured, and the $\epsilon_{11} = 4.514$ ²²

**Much higher capacitance values are attributed to the larger top contact area of these devices, compared to other nanowire-based VINGs.

The upper panel of Figure 6(a) displays the charge response from the VINGs with an active region consisting of N-polar GaN nanowires (GaN-NW-01) and Al-polar AlN nanowires (AlN-NW-01). The sinusoidal excitation force (lower panel) has a preload F_{dc} of 4.25 N, an amplitude (F_{ac}) of 440 mN and is applied at a frequency (f) of 30 Hz. In Figure 6(b), the normalized charge amplitude (q_{pz}^n) and phase in response to the force excitation are plotted as a function of frequency. The q_{pz}^n is interpreted as $d_{33,eff}$ along the c-axis of the wurtzite nanowires, considering that the force was applied in this direction. The extracted values are approximately 2.34 pC/N for AlN-NW-01 and 0.84 pC/N for GaN-NW-01. The observed 0° and 180° phase shifts are consistent with the Al- and N-polarity of the nanowires, perfectly aligning with the result of the bulk GaN substrate presented in Section 3.1. We further investigate a variety of AlN nanowire-based VINGs and summarize the signal output in Table 1. We systematically found lower values of $d_{33,eff}$ for the VINGs compared to the d_{33} of the single crystal substrate counterpart⁴, which is attributed to the reduced volume of piezoelectric material in a nanowire-based composite layer^{22,40,41}. In addition, the presence of the remaining h-PDMS layer on top of the nanowires leads to a degree of signal loss⁴². Although the studied AlN nanowire-based VINGs were made from the AlN nanowires grown under the same condition, we observed a variation of $d_{33,eff}$ in the range of 0.65 - 2.34 pC/N. This discrepancy is ascribed to device geometry fluctuations which depend on various parameters, including contact size, composite thickness, encapsulation quality, electrical contact quality, and self-assembly nature of the nanowires.

The normalized voltage amplitude $V_m^n(\omega)$ and phase response in Figure 6(c) exhibit a high-pass characteristic, which are similar to that observed in the GaN bulk substrate. The extracted $V_m^n(\omega)$ from equation (3) demonstrates good agreement with the detected piezo-voltages for all VINGs studied in this work. As examples, the extracted $V_m^n(\omega)$ from GaN-NW-01 and AlN-NW-01, represented as grey solid lines, are compared with the measured values in Figure 6(c). Table 1 reveals the difference between V_{sat}^n and V_{pz}^n when the device capacitance, C_{pz} , is much lower than that of the detection circuit, which is 20 pF in this set of experiments. This result unveils the impact of measurement configuration on piezo-voltage signal. Furthermore, we apply equation (5) using the measured value of V_{sat}^n to calculate q_{pz}^n , with the known impedances of our DUTs and detection circuit. These values are consistent with the measured $d_{33,eff}$ in Table 1. This approach provides an alternative method for deducing the $d_{33,eff}$ of the DUTs from their piezo-voltage, without directly measuring the generated charges.

To assess III-N nanowire VINGs for sensors and energy harvesters, we determine the corresponding FoM by calculating $g_{33,eff} = \frac{d_{33,eff}}{\epsilon_{33,eff}}$ (for sensing) and the product $g_{33,eff} \cdot d_{33,eff}$ (for energy harvesting), where $\epsilon_{33,eff}$ is the effective dielectric permittivity. In our experiments, the $\epsilon_{33,eff}$ cannot be accurately extracted from the impedance analyses because the device geometry cannot be precisely defined. Hence, we derive the $\epsilon_{33,eff}$ from a simplified model of a composite layer^{40,41}; see supplementary information. The lower $\epsilon_{33,eff}$ of approximately $3 \cdot \epsilon_0$ for the h-PDMS encapsulated AlN and GaN nanowires is able to counterbalance the reduction of $d_{33,eff}$ of the composite layer. Consequently, the $g_{33,eff}$ piezoelectric voltage coefficient of the nanowire-based VINGs remain promising compared to the other bulk materials examined. Table 1 shows that the $g_{33,eff}$ of the AlN nanowire-based VINGs generally surpasses those of single crystal

GaN and quartz bulk substrates as well as a sputtered AlN layer, indicating their advantage for mechanical sensing applications. On the other hand, the $d \cdot g$ energy harvesting figure of merit suggests that the AlN nanowire-based VINGs can offer a comparable power output, but it remains to be improved in comparison to AlN single crystal. It is important to note that a bending motion of the nanowires is not fully achieved in our experiments, thereby limiting the potential benefits from their inherent flexibility. The bending of nanowires could potentially yield a greater level of charge generation for the same applied force. For example, we have observed $d_{33,eff}$ of GaN and AlN nanowire-based VINGs up to 4 pC/N and 6 pC/N, respectively, which might be ascribed to the bending of the nanowires. These results will be further investigated in more detail. This higher-than-the-bulk value of the piezoelectric charge constant should extend the FoM for both sensing and harvesting beyond its bulk counterpart, which underscores the capability of nanowires as flexible piezoelectric nanogenerators.

Finally, as mentioned in Section 1, most piezo-voltage analyses of nanowire-based VINGs in the literature are performed through intermittent pressing on the devices. Here, in Figures 7(a)-(c), we present the charge and voltage response of AlN nanowire-based VINGs (AlN-NW-03) plotted as a function of time when subjected to a step-like force excitation. The force shown in Figure 7(c) has a preload of 3.5 N, an amplitude of 400 mN, and a frequency of 1 Hz. Figure 7(a) depicts negative and positive charge signals, when the DUTs was compressed or released, respectively. The sign of the signal is consistent with the Al-polarity of the nanowires. Ideally, the charge signal should remain at $-q_{pz}$ or $+q_{pz}$ when the DUTs are constantly compressed or released, respectively. The signal decay is caused by a quasi-static detection mode of the charge amplifier, which has the decay time of 1 second in this measurement. By dividing the charge variation (ΔQ) with the force variation (ΔF), we obtain $\frac{\Delta Q}{\Delta F} = 1.25$ pC/N, which is in agreement with the $d_{33,eff}$ of this device.

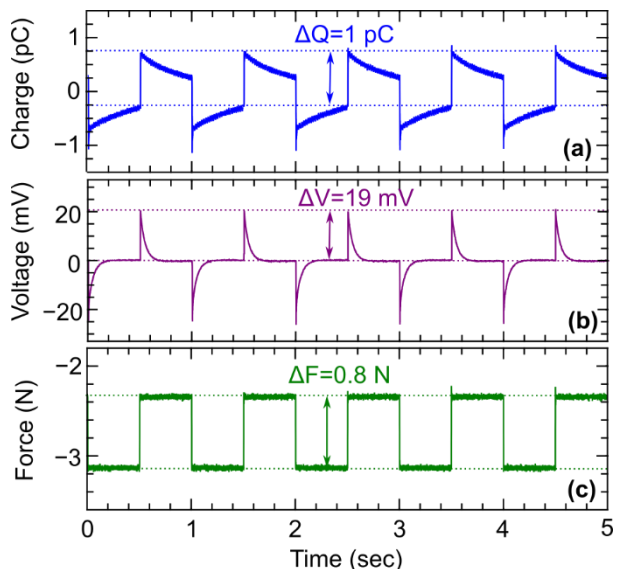


Figure 7 (a) Charge and (b) voltage signal from the AlN nanowire VINGs (AlN-NW-03) under a step-like force excitation at 1 Hz, as shown in (c).

Regarding the piezoelectric voltage signal, voltage spikes ($V_m(t)$) with amplitudes of $-V_0$ or $+V_0$ were observed when the

DUTs were compressed or released, respectively, as shown in Figure 7(b). The voltage variation (ΔV) and decay time (τ) can be determined from the following equation.

$$V_m(t) = \Delta V_0 e^{-\frac{t}{\tau}} \quad (6)$$

By fitting equation (6) with the results in Fig.7(b), the normalized voltage amplitude ($\Delta V_0/\Delta F$) and τ are approximately 24 mV/N and 45 milliseconds, respectively. Since $R_o \gg R_L$ in this device, a C_{tot} of 45 pF can be calculated from the relation $\tau = R_L \cdot C_{tot}$, allowing us to determine the $d_{33, eff}$ from equation (5). The obtained value is approximately 1.1 pC/N, slightly lower than the value from the charge measurement (1.27 pC/N). This discrepancy is attributed to the finite detection bandwidth of the voltage amplifier and the limited precision of our measurement setup. Nevertheless, it remains a relatively reliable indication of the generated charge from the devices and is an alternative approach for measurement of the piezoelectric charge coefficients.

Conclusions and Remarks

In this work, a detailed analysis of direct piezoelectric response, including the piezo-charge and piezo-voltage of AlN nanowire-based VINGs are performed as a function of mechanical excitation frequency. The piezo-charge, piezo-voltage, and impedance of the devices are able to be directly correlated by using an equivalent circuit model. We experimentally demonstrate that comparing solely the absolute values of piezo-voltages from different prototypes can lead to an erroneous interpretation of device performance since such values can vary with testing configurations. We also show that the piezo-voltage is also influenced by the device impedance, which can depend on a variety of parameters. Therefore, it is more reliable to extract the g piezoelectric voltage coefficient and the product $d \cdot g$, both representing important figures of merit of piezoelectric materials, to evaluate and compare the device's performance. The piezoelectric g coefficient determined from our results reveal that nanowire-based VINGs can potentially outperform their rigid counterparts for mechanical sensing

applications, while their capability of energy generation remains to be improved. In addition, without directly measuring the piezoelectric charges generated by the devices, we also present alternative possibilities to deduce the $d_{33, eff}$ using the piezoelectric volage and the impedances of the device, along with a detection circuit. This work provides an experimental guideline and protocol not only for understanding the characteristics of VINGs, but also for facilitating a quantitative comparison between nanostructured piezoelectric sensing and energy harvesting devices.

Credit authorship contribution statement

N. Buatip: Device design and fabrication, Process optimizations Investigation, Methodology, editing manuscript, T. Auzelle: III-N nanowires growth, Conceptualization, Funding acquisition, P. John: III-N nanowires growth, Conceptualization, M. Sohdi and M. Saluan: PDMS optimization, B. Fernandez: Device fabrication, D. Mornex: Technical support for setup development, E. Monroy: GaN nanowires growth, editing manuscript, C. R. Bowen: Review and editing manuscript. S. Rauwerdink: Sputtering AlN layers, R. Songmuang: Writing, Data curation, Methodology, Investigation, Setup development, Conceptualization, Funding acquisition.

Declaration of Competing Interest

The authors have no conflicts of interest.

Acknowledgment

We acknowledge the assistance from Nanofab/Néel Institute for sample fabrications and from SERAS/Néel Institute for the set-up development. The work is financially supported by ARC-Energy project, GaNEX, ANR-15-IDEX-02, ANR-PRCI NanoFlex (Project No. ANR-21-CE09-0044), and German Bundesministerium für Bildung und Forschung (Project No. FKZ:13N13662).

Keywords

Piezoelectric nanogenerators, III-Nitrides, nanowires, piezoelectric constants, energy harvesters

¹ Z. L. Wang and J. Song, Piezoelectric nanogenerators based on zinc oxide nanowire arrays, *Science* 312 (2006) 242–246.

² Z. L. Wang, Nanogenerators for Self-powered Devices and Systems, <http://hdl.handle.net/1853/39262>.

³ F. Bernardini, V. Fiorentini, and D. Vanderbilt, Spontaneous polarization and piezoelectric constants of III-V nitrides, *Phys. Rev. B* 56 (1997) R10024(R).

⁴ O. Ambacher, J. Majewski, C. Miskys, A. Link, M. Hermann, M. Eickhoff, M. Stutzmann, F. Bernardini, V. Fiorentini, V. Tilak, B. Schaff, and L. F. Eastman, Pyroelectric properties of Al(In)GaN/GaN hetero- and quantum well structures, *J. Phys. Condens. Matter* 14 (2002) 3399.

⁵ M.J. Krasny and C.R. Bowen, A system for characterisation of piezoelectric materials and associated electronics for vibration powered energy harvesting devices, *Measurement* 168 (2021) 108285.

⁶ J. Briscoe, N. Jalali, P. Woolliams, M. Stewart, P. M. Weaver, M. Cain and S. Dunn, Measurement techniques for piezoelectric nanogenerators, *Energy Environ. Sci.* 6(2013) 3035-3045

⁷ D. B. Deutz, J.-A. Pascoe, B. Schelen, S.van der Zwaag, D. M. de Leeuwa and P. Groenae, Mater. Horiz. Analysis and experimental validation of the figure of merit for piezoelectric energy harvesters 5 (2018) 444.

⁸ X. Xu, A. Potié, R. Songmuang, J. W. Lee, B. Bercu, T. Baron, B. Salem and L.t Montè, An improved AFM cross-sectional method for piezoelectric nanostructures properties investigation: application to GaN nanowires, *Nanotechnology* 22 (2011) 105704.

⁹ N. Gogneau, N. Jamond, P. Chrétien, F. Houzé, E. Lefeuvre, and M. Tchermysheva, From single III-nitride nanowires to piezoelectric generators: New route for powering nomad electronics, *Semicond. Sci. Technol.* 31 103002 (2016).

¹⁰ W. Zhao, P. Xumin, H. Yahua, H. Yongming, G. Haoshuang, and W. Yu, Piezoelectric Nanowires in Energy Harvesting Applications, *Adv. Mater. Sci. Eng.*, 2015 (2015) 165631

¹¹ X. Zhang, J. Villafuerte, V. Consonni, J.-F. Capsal, P.-J. Cottinet, L. Petit, and M.-Quyen Le, Characterizing and Optimizing Piezoelectric Response of ZnO Nanowire/PMMA Composite-Based Sensor, *Nanomaterials* 11 (2021) 1712.

¹² X. Zhang, M.-Quyen Le, O. Zahhaf, J.-F. Capsal, P.-J. Cottinet, and L. Petit, Enhancing dielectric and piezoelectric properties of micro-ZnO/PDMS composite-based dielectrophoresis, *Materials and Design* 192 (2020) 108783.

¹³ G. Gautschi, Piezoelectric Sensories Force, Strain, Pressure, Acceleration and Acoustic Emission Sensors Materials and Amplifiers, Springer-Verlag Berlin Heidelberg New York in 2002

- ¹⁴A. Šutka, P. C. Sherrell, N. A. Shepelin, L. Lapčinskis, K. Mālnieks, and A.V. Ellis, Measuring Piezoelectric Output—Fact or Friction? *Adv. Mater.* 32(2020) 2002979.
- ¹⁵D. Berlincourt and H. A. Krueger, Domain processes in Lead Titanate Zirconate and Barium Titanate Ceramics, *J. Appl. Phys.* 30 (1959) 1804-1810.
- ¹⁶<https://www.piezotest.com/> (02/02/2024)
- ¹⁷M. Stewart, M. Battrick, and M.G. Cain, Measuring piezoelectric d_{33} coefficients using the direct method, NPL, Teddington, Measurement good practice guide No. 44, Jun. 2001.
- ¹⁸M. Stewart and M. G. Cain, Direct Piezoelectric Measurement: The Berlincourt Method. In M. Cain (eds) *Characterisation of Ferroelectric Bulk Materials and Thin Films*. Springer Series in Measurement Science and Technology, vol 2. Springer-Verlag, (2014).
- ¹⁹S. Xu, Y. Qin, C. Xu, Y. Wei, R. Yang and Z. L. Wang, Self-powered nanowire devices, *Nat. Nanotechnology* 5(2010) 366–373.
- ²⁰K. Uchino Piezoelectric Energy Harvesting Systems—Essentials to Successful Developments, *Energy Technol.* 6(2018) 829 – 848.
- ²¹P. Muralt, Piezoelectric thin film for MEMs, *Integr. Ferroelectr.* 17(1997) 297.
- ²²J. Tichý, J. Erhart, E. Kittinger, and J. Přívratská, *Fundamentals of Piezoelectric Sensorics: Mechanical, Dielectric, and Thermodynamical Properties of Piezoelectric Materials*, Springer, Berlin, Heidelberg (2010).
- ²³R. Songmuang, O. Landré, and B. Daudin, From nucleation to growth of catalyst-free GaN nanowires on thin AlN buffer layer, *Appl. Phys. Lett.* 91 (2007) 251902.
- ²⁴M. Azadmand, T. Auzelle, J. Lähnemann, G. Gao, L. Nicolai, M. Ramsteiner, A. Trampert, S. Sanguinetti, O. Brandt, and L. Geelhaar, Self-Assembly of well-Separated AlN nanowires directly on sputtered metallic TiN films, *Phys. Status Solidi RRL* 14 (2020) 1900615.
- ²⁵P. John, M. Gómez Ruiz, L. van Deurzen, J. Lähnemann, A. Trampert, L. Geelhaar, O. Brandt and T. Auzelle, Growth kinetics and substrate stability during high-temperature molecular beam epitaxy of AlN nanowires, *Nanotechnology* 34 (2023) 465605
- ²⁶L. Jaloustre, S. Le Denmat, T. Auzelle, M. Azadmand, L. Geelhaar, F. Dahlem, and R. Songmuang, Toward quantitative measurements of piezoelectricity in III-N semiconductor nanowires, *ACS Appl. Nano Mater.* 4 (2021) 43–52.
- ²⁷M. den Hertog, F. Gonzalez-Posada, R. Songmuang, J.-L. Rouviere, T. Fournier, B. Fernandez, and E. Monroy, Correlation of polarity and crystal structure with optoelectronic and transport properties of GaN/AlN/GaN nanowire sensors, *Nano Lett.* 12 (2012) 5691–5696.
- ²⁸A. Ibanez and M. Salaiün: Method for densely filling micrometric or sub-micrometric inter-wire spaces with an organosilicated hybrid matrix and composite device thus obtained, WO/2023/111477, (2023)
- ²⁹P. Sundriyal, M. Pandey, and S. Bhattacharya, Plasma-assisted surface alteration of industrial polymers for improved adhesive bonding, *Int J Adhes Adhes.* 101 (2020) 102626.
- ³⁰T. Ikeda, *Fundamentals of Piezoelectricity*, Oxford university press (1990)
- ³¹B. Jaffe, W. R. Cook Jr. and H. Jaffe, “Piezoelectric Ceramics,” Academic Press, London and New York (1971).
- ³²C. M. Lueng, H. L. W. Chan, C. Surya, and C. L. Choy, Piezoelectric coefficient of aluminum nitride and gallium Nitride, *J. Appl. Phys.*, 88 (2000)5360.
- ³³J. Karki, Signal Conditioning Piezoelectric Sensors Application Report: <https://www.ti.com/lit/an/sloa033a/sloa033a.pdf>
- ³⁴A. L. Kholkin, Ch. Wutchrich, D. V. Taylor, and N. Setter, Interferometric measurements of electric field-induced displacements in piezoelectric thin films. *Rev. Sci. Instrum.* 67(1996) 1935-1941.
- ³⁵I. L. Guy, S. Muensit, and E. M. Goldys, Extensional piezoelectric coefficients of gallium nitride and aluminum nitride, *Appl. Phys. Lett.* 75 (1999) 4133-4135.
- ³⁶V.E. Bottom, Measurement of the Piezoelectric Coefficient of Quartz Using the Fabry-Perot Dilatometer, *J. Appl. Phys.* 41 (1970) 3941–3944.
- ³⁷M. Prokic, *Piezoelectric transducers and modelling*, MP Interconsulting (2004)
- ³⁸Y. Su, C. Dagdeviren, and R. Li, Measured output voltages of piezoelectric devices depend on the resistance of voltmeter, *Adv. Funct. Mater.* 25 (2015) 5320.
- ³⁹M. H. Amiri, R. Fatscher, R. Taylor, P. R.F. Rocha, C. R. Bowen, K. Asad, Piezoelectric energy harvesters: A critical assessment and a standardized reporting of power-producing vibrational harvesters, *Nano Energy* 106 (2023) 108073.
- ⁴⁰W. A. Smith and B.A. Auld, Modeling 1-3 Composite Piezoelectrics: Thickness-Mode Oscillations, *Trans. Ultrason., Ferroelectr. Freq. Control* 38 (1991) 40-47.
- ⁴¹N. Doumit and G. Poulin-Vittrant, Effect of the dielectric and mechanical properties of the polymer matrix on ZnO-nanowire-based composite nanogenerators performance, *Adv. Theory Simul.* 3 (2020) 2000128.
- ⁴²R. Hinchet, S. Lee, G. Ardila, L. Montès, M. Mouis, and Z. L. Wang, Performance optimization of vertical nanowire-based piezoelectric nanogenerators, *Adv. Funct. Mater.* (2013)1.